Biosystems Engineering 246 (2024) 191–203

Contents lists available at ScienceDirect

Biosystems Engineering

journal homepage: www.elsevier.com/locate/issn/15375110

Research Paper

# Development of a microwave sensor for the non-invasive detection of plant responses to water stress: A practical application on maize (*Zea mays* L.)

Valeria Lazzoni [a,*], Danilo Brizi [a], Nicolina Staglianò [b], Cristiana Giordano [c], Elisa Pecoraro [c], Monica Anichini [c], Francesca Ugolini [c], Marco Bindi [b], Giovanni Argenti [b], Agostino Monorchio [a], Riccardo Rossi [b]

[a] University of Pisa, Department of Information Engineering, Pisa, 56122, Italy
[b] Department of Agriculture, Food, Environment and Forestry (DAGRI), University of Florence, Piazzale delle Cascine 18, 50144, Florence, Italy
[c] Institute of BioEconomy of the National Research Council (CNR-IBE), via Madonna del Piano 10, 50019, Sesto Fiorentino il, Italy

ARTICLE INFO

*Keywords:*
Drought stress
Stem histology
Wireless sensors
Microwaves
Q-factor

ABSTRACT

In this study, a novel microwave sensing system, consisting of a microstrip self-resonant spiral coil inductively coupled to an external concentric planar probe loop, is presented and applied to the non-destructive detection of morpho-physiological plant responses to water stress. The optimised set-up of the proposed sensor ensures a highly sensitive spiral coil, which is a fundamental requirement to derive accurate information on plants' behavioural alterations related to water stress conditions. The proposed microwave sensor was tested it on two potted maize cultivars (*Zea mays* L.), namely "*Cinquantino Bianchi*" (*CB*) and "*Scagliolo Frassine*" (*SF*). For each cultivar, half of the samples were maintained at 100% (T100) field capacity while the other half was at 25% (T25) from 46 to 74 Days After Sowing (DAS). The frequency ($f_r$) shift and the amplitude peaks variation of the real component of the external planar probe input impedance ($\Re(Z_{input})$) were obtained daily by positioning the sensor on the stem. These measured data were related to morpho-physiological parameters destructively acquired at four different growth stages. The resulting linear correlation between the stem's freshwater content ($FWC_{stem}$) with both $f_r$ ($r > -0.64$) and the amplitude peaks ($\Re(Z_{input})$) ($r > -0.70$) provided evidence of the sensor's ability to identify stem dielectric properties' variations between the two water treatments. Concurrently, the sensor response demonstrated the capability to identify changes in the morphology and histology of the stem. Based on preliminary findings, the proposed sensor shows potential for employment in the real-time monitoring of plant water status, contributing to more economically and environmentally sustainable crop management practices. While the current correlations between plant water content and sensor measurements require further refinement to meet the rigorous industrial standards, nevertheless a large-scale adoption can be envisioned by leveraging IoT methodologies.

Nomenclature

| | |
|---|---|
| *AVG TR* | Average transpiration rate [g] |
| *C* | Capacitance [F] |
| $D_x$ | Diameter of the x-th part of the stem [m] |
| *DAGB* | Dry Above-Ground Biomass [g] |
| *DBGB* | Dry Above-Ground Biomass [g] |
| *DAS* | Day After Sowing |
| $DWC_x$ | *x* dry base water content [%] |
| *EM* | Electromagnetic |
| *EPE foam* | Expanded Polyethylene |
| $f_r$ | Resonant frequency [Hz] |
| *FAGB* | Fresh Above-Ground Biomass [g] |
| *FBGB* | Fresh Below-Ground Biomass [g] |
| *FDR* | *x* fresh base water content [%] |
| *FTIR-ATR* | Attenuated total reflectance Fourier transform mid-infrared |
| $FWC_x$ | 100% Field Capacity |

(continued on next column)
(continued)
(continued on next page)

* Corresponding author.
*E-mail addresses:* valeria.lazzoni@phd.unipi.it (V. Lazzoni), danilo.brizi@unipi.it (D. Brizi), nicolina.stagliano@unifi.it (N. Staglianò), cristiana.giordano@ibe.cnr.it (C. Giordano), elisa.pecoraro@ibe.cnr.it (E. Pecoraro), monica.anichini@ibe.cnr.it (M. Anichini), francesca.ugolini@ibe.cnr.it (F. Ugolini), marco.bindi@unifi.it (M. Bindi), giovanni.argenti@unifi.it (G. Argenti), agostino.monorchio@unipi.it (A. Monorchio), r.rossi@unifi.it (R. Rossi).

https://doi.org/10.1016/j.biosystemseng.2024.08.007
Received 15 February 2024; Received in revised form 1 July 2024; Accepted 8 August 2024
Available online 13 August 2024

(*continued*)

| | |
|---|---|
| *H-field* | Reactive Magnetic Field [A $m^{-1}$] |
| $H_2O_x$ | $x$ water content [g] |
| *IE* | Interdigitated-Electrodes |
| *L* | Inductance [H] |
| *LWS* | Leaf Wetness Sensors |
| *M* | Inductive Mutual Coupling [H] |
| *PA* | Precision Agriculture |
| *PCA* | Principal Component Analysis |
| *PCB* | Printed Circuit Board |
| *PDMC* | Percentage Dry Matter Content [%] |
| *PVC* | Polyvinyl Chloride |
| $Q_{factor}$ | Quality Factor [N/A] |
| *R* | Resistance [Ω] |
| *RFID* | Radio Frequency Identification |
| *SH* | Stem Height [m] |
| *SMA* | Sub Miniature version A |
| *SV* | Stem volume [$cm^3$] |
| *T100* | 100% Field Capacity |
| *T25* | 25% Field Capacity |
| *TDR* | Time Domain Reflectometry |
| tan$\delta$ | Dielectric Loss Tangent [N/A] |
| *UAV* | Unmanned Aerial Vehicle |
| *VNA* | Vector Network Analyzer |
| $Z_{input}$ | Input Impedance [Ω] |
| $Z_{probe}$ | Stand-alone probe loop impedance [Ω] |
| $\varepsilon$ | Dielectric Permittivity |
| $\varepsilon_0$ | Vacuum Dielectric Permittivity [$F\,m^{-1}$] |
| $\omega$ | Angular Frequency [Rad $s^{-1}$] |
| $\Psi_{min}$ | Minimum leaf water potential [bar] |
| $\rho_{stem}$ | Stem density [g $cm^{-3}$] |
| $\sigma$ | Conductivity [S $m^{-1}$] |
| $\Re\ (Z_{input})$ | Maximum of the real part of the input impedance [Ω] |

## 1. Introduction

The Intergovernmental Panel on Climate Change (2023) forecasts more frequent and severe extreme weather events, exacerbating water scarcity and threatening global food security through diminished crop yields (Kulundžić et al., 2021; Pawlak and Kołodziejczak, 2020). This context underscores the urgent need for innovative agricultural technologies aimed at enhancing water resource management and crop productivity. Precision agriculture (PA) emerges as a pivotal approach in this regard, offering strategies to optimise yields with minimal inputs by leveraging advanced technologies for real-time monitoring and management of crop health and nutrition (Palazzi, Bonafoni, et al., 2019a). As such, PA techniques, including remote sensing and on-field technologies, are at the forefront of research to ensure food security against the backdrop of climate change.

Satellite- and unmanned aerial vehicle (UAV)-based remote sensing is beneficial for collecting high-resolution information over large crop stand areas by multiple sensors, such as visible, multi-, hyper-spectral and thermal cameras (Brocca et al., 2018; Mulla, 2013; Zhang et al., 2020). However, remote sensing is largely dependent on cloud cover and weather conditions which often limits its operability and temporal resolution, hindering continuous monitoring, which is essential for effective crop and water resource management. Moreover, most optical imaging techniques do not allow detection of crop nutritional deficiencies before visual symptoms become noticeable, i.e. when damages have already happened, as their spatial resolution and/or the spectral information are often not suitable for this purpose (Palazzi, Bonafoni, et al., 2019a).

Conversely, sensors installed in-field have the potential to be a smart farming solution for indirectly and/or directly assessing the crop status due to their decreasing cost per unit and the ability to continuously collect real-time data regardless of environmental perturbations. At present, several tools are available for monitoring plant responses to external stimuli (e.g., water shortage) at a fine spatial-temporal scale, including soil and *in-vivo* sensors. Soil electromagnetic (EM) sensors operate on the assumption that the EM wave propagation in bulk soil is principally governed by liquid water, which possesses a significantly larger dielectric permittivity ($\varepsilon_r$) than the other components (gaseous air and solid soil minerals). A range of techniques, including time domain reflectometry (TDR), frequency domain reflectometry (FDR), and radio frequency identification (RFID), have been developed to record signals especially for indirectly defining water shortages in crop plants (Adelakun and Sri Ranjan, 2013; Majcher et al., 2020; Woszczyk et al., 2019). Nevertheless, the cost and requirements for waveforms analysis could limit the widespread application of TDR in appropriately scheduling the irrigation. At the same time, FDR also requires careful installation to avoid air gaps between the sensor and the soil and is generally limited to use in non-saline soils (Hardie, 2020). To overcome these problems, two macro groups of RFID sensors were developed: chip-provided (Boada et al., 2018; Cappelli et al., 2021; da Fonseca et al., 2017; Daskalakis et al., 2016; Deng et al., 2020; Pichorim et al., 2018; Wang et al., 2020) and chipless versions (Chan et al., 2022; Costa et al., 2019; Gopalakrishnan et al., 2021, 2022; Martuza et al., 2018; Salmerón et al., 2018). Most chip-provided RFID equipment are characterised by an unacceptable high cost of manufacturing and assembly, due to the presence of electronics. Furthermore, harmful chemicals could leak from integrated circuits, polluting the soil and water and jeopardising the regular growth cycle of cultivated plants. On the other hand, the lack of batteries and electronic circuits in chipless RFID allows an advantageous reduction of the overall cost of the technology and achieves a theoretically unlimited lifespan, resulting in a sensor that is suitable for safe use in different environmental conditions (Costa et al., 2021; Gopalakrishnan et al., 2022). Despite their proven potential for application in agricultural water management, soil sensors only offer an indirect overview of the plant status. They cannot provide quantitative insights into the complex metabolic responses of plants to drought at a single-organ level, which is desired for setting-up irrigation that responds to the real plant needs.

*In-vivo* sensors which can be applied directly to plant tissues or organs are powerful alternatives for determining the actual plant water status with high accuracy. In the literature, different studies have investigated plant water stress using leaf sensors (Dadshani et al., 2015; Daskalakis et al., 2018; Dey et al., 2020; Hornero et al., 2017; Palazzari et al., 2015; Palazzi, Bonafoni, et al., 2019a; Yan et al., 2020). Furthermore, these sensors have been employed to monitor the temperature disparity between the leaf and the surrounding air (Daskalakis et al., 2018; Palazzari et al., 2015; Palazzi, Bonafoni, et al., 2019b). This difference is strictly related to the plant water stress, and it can be used as a decision parameter in a local irrigation system. Nevertheless, the employment of an electrical circuit for the power supply and transmission of sensor data is the primary drawback of these applications, as in the case of chip-provided devices. This results in an increase in the sensor price, the impossibility of outdoor usage, and a shorter lifespan. The aforementioned leaf sensors exhibit distinct characteristics in comparison to leaf wetness sensors (LWS). Indeed, these sensors are able to detect leaf wetness and turgidity (moisture level), which can be attributed to various factors, including the presence of dew, fog, rain, and irrigation. Currently, various solutions can be found on the market (AgriHouse Inc. (2017); Decagon Devices Inc (2016)) but the high price makes their practical application challenging for farmers.

An additional category of *in vivo* sensors includes stem sensors, physically inserted into the plant tissue. These sensors have been tested in monitoring the water flow dynamics of olive trees (Comparini et al., 2020), tomato (Janni et al., 2019) and tobacco plants (Garlando et al., 2022). In particular, these manuscripts show a multi-electrode approach to measuring the stem electrical resistance in plants subjected to different water stress treatments. Physiological parameters and electrical activity have been correlated, highlighting the possibility of differentiating the electric signals related to drought conditions of different intensity. However, inserting electrodes into a plant can be invasive and may damage the plant tissues, potentially leading to tissue death or infection. Plants may allocate resources and energy towards

repairing or defending against this perceived threat, altering their physiological functions in the process. This can not only affect the plant's health but also introduce inaccuracies in the measurements and in data interpretation. Lastly, a non-invasive approach for quantifying stem water content and tracking its variation over time is reported in Cheng et al. (2021) using a frequency-domain dielectric sensor with an interdigitated-electrodes (IE) probe to detect change in the dielectric properties of the stems. These variations are subsequently transformed into a voltage output (mV) which serves as an indicator of the stem water content. However, this sensor necessitates a wired connection to a data acquisition system or to a measurement instrument in order to analyse the output voltage. This may introduce additional dependencies and requirements for data collection.

To overcome these limits, it becomes imperative to develop non-invasive, passive, and cost-effective sensors for monitoring the water status of individual plant organs. When strategically positioned on various plant organs, these sensors would offer the capability to continually track plant water status over extended periods without causing any harm or disruption. Their non-destructive nature may allow also for the unobtrusive observation of small deviations related to water stress, well before any visible symptoms manifest. Consequently, the implementation of such an early warning system holds the potential to inform agricultural practices proactively. This includes optimising irrigation schedules or making informed choices regarding drought-resistant crop varieties, thus underscoring the invaluable contribution of these sensors in advancing PA.

Following these observations, the present work aims to implement a non-invasive wireless, low-cost, passive and chipless microwave sensor based on an optimised self-resonant spiral for the real-time evaluation of the actual plant water status. The novel sensor was directly applied on the stem of two maize cultivars (*Zea mays* L.) with different development habits subjected to various irrigation treatments (100% and 25% of field capacity) and the acquired electromagnetic signal patterns were correlated with morpho-physiological, anatomical, and histochemical changes associated with early water stress responses.

## 2. Materials and methods

### 2.1. Sensor design

The proposed radiating system, operating at 600 MHz when positioned in open space, consists of a self-resonant microstrip planar spiral coil inductively coupled to a concentric and non-resonant actively fed RF probe loop (Fig. 1a). The inner spiral resonator is responsible for the overall sensing performance, whereas the external single probe loop (Fig. 1b) has the role to both feed the inner spiral sensor and to collect the resulting signal variation. The chosen operating frequency ensures high penetration depth as well as a high degree of downsizing, while preserving an acceptable level of sensitivity. With the aim of accomplishing these desired targets, the spiral sensor geometric characteristics were established by following a Q-factor maximisation procedure (Brizi et al., 2019). The Q-factor can be defined with the following equation:

$$Q_{factor} = \left.\frac{\omega L_{SS}}{R_{SS}}\right|_{\omega=\omega_{self-resonance}} \quad (1)$$

where $L_{SS}$ and $R_{SS}$ are respectively the inductance and the resistance of the spiral sensor (SS) at the operative frequency (i.e., 600 MHz).

As reported in the literature (Costa et al., 2019), $R_{SS}$ and $L_{SS}$ strongly depend on the geometric parameters of the sensor. Therefore, the spiral sensor output diameter (2 × R) was fixed at 18 mm according to the standard stem diameter of maize plants under different irrigation regimes (Sabiel et al., 2014). Subsequently, the inner radius (r), number of turns (N), metal line width (w), spacing between windings (s), and the conductor thickness were all determined to maximise the Q-factor parameter (Table 1).

In order to best feed the inner spiral sensor, the actively fed RF probe loop was designed as a single loop with an external diameter $(d_{probe})$ of 22 mm, a metal line width $(w_{probe})$ of 0.5 mm and a self-resonance frequency of approximately 1.67 GHz. The high self-resonance frequency guarantees that the probe loop behaves as a pure inductor at the operative frequency. Both the spiral sensor and the probe loop have been fabricated by exploiting Printed Circuit Board (PCB) technology. In order to better adapt the spiral sensor to curved surfaces (e.g., plant stem), a high structural flexibility was guaranteed by adopting a 0.1 mm thick FR4 dielectric substrate ($\varepsilon_r = 4.3$ and $\tan\delta = 0.025$) for the spiral resonator (Fig. 1c) and a standard (and rigid) 0.8 mm thick FR4 slab for the probe loop (Fig. 1d). Finally, a 50 Ω SubMiniature version A (SMA) connector was soldered to the probe loop in order to connect it to a

**Table 1**
Spiral sensor geometrical design characteristics.

| Parameters | Value |
|---|---|
| Conductor thickness | 0.35 μm |
| Inner radius | 0.6 mm |
| Metal line width | 0.6 mm |
| Number of turns | 6 |
| Output radius | 9 mm |
| Q factor | 391 |
| Spacing between windings | 1.4 mm |

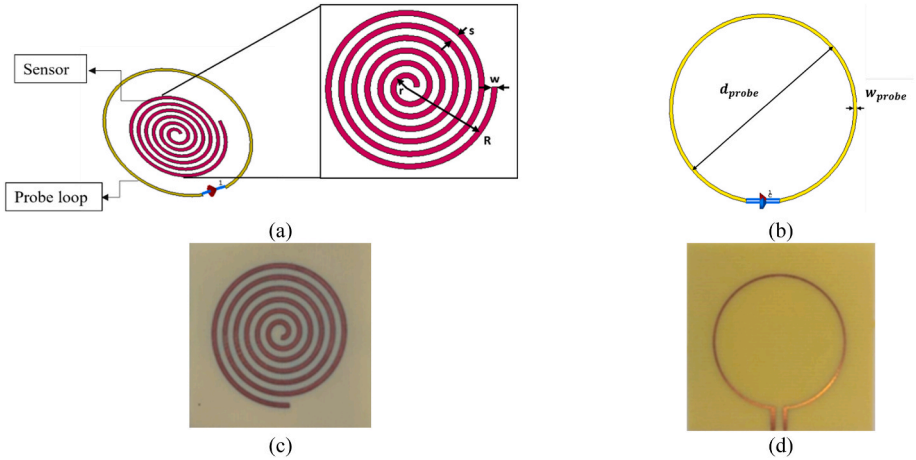


**Fig. 1.** (A) 3D CAD model of the described sensing system. The inner spiral sensor is inductively coupled with an external, unloaded probe loop; **(b)** probe loop CAD structure; **(c)** fabricated PCB spiral resonator, and **(d)** fabricated PCB probe loop.

Vector Network Analyzer (VNA).

### 2.2. Sensor operation and sensitivity

The idea behind the proposed system is to create a sensor extremely sensitive to changes in the plant tissues' electromagnetic properties in response to environmental challenges, including water stress. The inner spiral sensor is physically attached to the target sample and inductively coupled to the external probe loop (Fig. 2a). By reading the probe loop input impedance $Z_{input}$, it is possible to derive tissue status information from the spiral sensor's behaviour. In particular, hydric stress detection is based on the variation of the probe loop input impedance ($Z_{input}$) which is determined by changes in the spiral sensor lumped parameters ($R_{SS}$, $L_{SS}$ and $C_{SS}$) consequent to the tissues' dielectric properties variation due to water stress. According to Brizi et al. (2019), the equivalent circuit of the described configuration is depicted in Fig. 2b and the probe loop input impedance $Z_{input}$ can be expressed in the following form:

$$Z_{input} = R_{probe} + j\omega L_{probe} + \frac{\omega^2 M^2}{R_{SS} + j\omega L_{SS} + \frac{1}{j\omega C_{SS}}} \tag{2}$$

where $R_{probe}$ and $L_{probe}$ represent, respectively, the external probe loop resistance and inductance; $R_{SS}$, $L_{SS}$ and $C_{SS}$ indicate the spiral sensor resistance, inductance, and capacitance while $M$ denotes the inductive mutual coupling term between probe loop and spiral sensor.

As reported in previous studies (Eroglu et al., 2019; Sharma et al., 2020), the plant stems dielectric properties vary during the growth stage and depends on the health status of the plant. Therefore, a water stress condition leads to a volumetric water content decrease, which is responsible for lower dielectric permittivity and conductivity values. In more detail, considering a biological tissue, the dielectric permittivity can be expressed as a complex value:

$$\varepsilon = \varepsilon' + j\varepsilon'', \tag{3}$$

where the real term ($\varepsilon'$) represents the tissue relative dielectric constant and the imaginary term ($\varepsilon''$) represents the tissue losses. The imaginary term is strictly linked to the electrical conductivity σ (S $m^{-1}$):

$$\sigma = \omega \varepsilon_0 \varepsilon'', \tag{4}$$

where $\varepsilon_0 = 8.85^{*}\ 10^{-12}\ (F\,m^{-1})$ is the vacuum dielectric permittivity and $\omega$ (rad $s^{-1}$) is the considered pulsation.

To describe the performance of the spiral sensor as a function of the dielectric characteristics of the examined tissue, an analytical model is developed. To replicate a realistic scenario in which the sensor is attached to the plant stem, it is possible to adopt a simplified model in which the space beneath the spiral sensor consists of biological tissue while, on the opposite side, only air is present (Fig. 2a). Therefore, the equivalent permittivity experienced by the sensor can be approximated by the average value of the complex dielectric permittivity of the tissue, related to the water stress condition, and the permittivity of air (Eq. (5)):

$$\varepsilon_{eff} = \frac{\varepsilon_{tissue} + \varepsilon_{air}}{2}. \tag{5}$$

This permittivity value ( $\varepsilon_{eff}$) will affect the capacitive behaviour of the spiral sensor by directly multiplying the capacitance value $C_{SS}$ (Eq. (6)).

$$C_{eff} = \varepsilon_{eff} C_{SS}. \tag{6}$$

By replacing Eq. (6) in (2), the probe loop input impedance $Z_{input}^{eff}$ is obtained (Eq. (7)):

$$Z_{input}^{eff} = R_{probe} + j\omega L_{probe} + \frac{\omega^2 M^2}{R_{eff} + j\omega L_{SS} + \frac{1}{j\omega C_{eff}}}, \tag{7}$$

where $R_{eff}$ and $C_{eff}$ can be described as reported in Eq. (8).

$$\begin{cases} R_{eff} = R_{SS} + \dfrac{\varepsilon''_{eff}}{\omega C_{SS}\left(\varepsilon''_{eff}{}^2 + \varepsilon'_{eff}{}^2\right)} \\ C_{eff} = C_{SS}\dfrac{\left(\varepsilon''_{eff}{}^2 + \varepsilon'_{eff}{}^2\right)}{\varepsilon'_{eff}} \end{cases}. \tag{8}$$

As can be inferred from Eq. (8), the tissue dielectric properties influence the system performance. In particular, when the effective resistance $R_{eff}$ changes under different stem dielectric properties, then a corresponding increment or reduction of the amplitude peaks of the input impedance real component occurs. Conversely, an effect on the equivalent capacitance $C_{eff}$ is related to a change in the resonant frequency (that is visible in a frequency shift of the impedance peak of the probe loop input impedance).

To validate the system effectiveness in monitoring the plant health

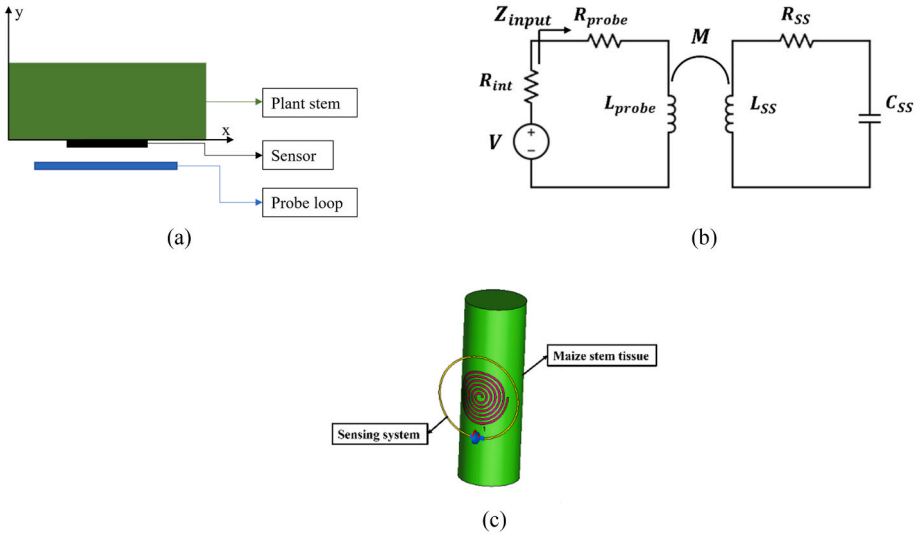


**Fig. 2.** (A) Pictorial representation of the proposed sensing system set-up; **(b)** corresponding equivalent circuit: the non-resonant probe loop (left side) is mutually coupled with the inner spiral sensor (right side); **(c)** numerical CAD model: the single probe loop is actively feeding the spiral sensor positioned on the maize stem tissue.

status, a numerical set-up was conceived by using the electromagnetic full-wave software CST Studio Suite-Simulia® (Dassault Systèmes®, Vélizy-Villacoublay, France) based on the Finite Element Method. Firstly, the input impedance of the stand-alone probe loop was evaluated to investigate if its self-resonance frequency, after the introduction of the 50-Ω connector soldering, are out of the operating frequency range (100–700 MHz). To simulate the soldering effect, a parasitic capacitance ($C_{parasitic} = 1.31\ pF$) has been introduced in parallel to the feeding port.

Secondly, a reasonable estimate of the maize stalk material permittivity is needed before numerical simulations can be performed. A study by Ulaby and El-rayes (1987) found that maize stalk permittivity ranges from 2 to 40 within the frequency range from 1.5 to 8 GHz. As expected, the permittivity increases with higher water content. Similar results were found by another study (Sharma et al., 2020) that measured the stalk maize section's permittivity as between 10 and 40 at 1.25 GHz. Based on these studies and knowing that the permittivity is higher at lower frequencies, to model a healthy maize stalk it was decided to use permittivity ($\varepsilon'$) and conductivity ($\sigma$) values respectively of 60 and 1.5 ($Sm^{-1}$) at the selected operating frequency range. To simulate a maize stalk, a cylinder was realised and placed into contact with the sensor (Fig. 2c). The cylinder dimensions have been selected as r = 10 mm and h = 60 mm in order to be comparable with the sensor sensing penetration depth.

By progressively decreasing maize tissue dielectric properties from $\varepsilon' = 60$ and $\sigma = 1.5$ ($Sm^{-1}$) (water stress status 1) to $\varepsilon' = 10$ and $\sigma = 0.1$ ($Sm^{-1}$) (water stress status 7), different water stress states were simulated. The dielectric properties, used in each numerical simulation, are reported in Table 2. To monitor the health condition, the resonant frequency shift and the peak amplitude of the input impedance real part were evaluated. In the following section, the accuracy of the results will be discussed.

### 2.3. Plant material and experimental design

The microwave sensing experiments were conducted on a monocotyledonous crop species (*Zea mays* L.). Indeed, monocots typically lack secondary tissue growth from the vascular cambium, which ensures that the sensor response reaches the composition of the primary structure (i.e., rind, pith and vascular bundles). Two maize cultivars, namely "Cinquantino Bianchi" (CB) and "Scagliolo Frassine" (SF), were used in this study (54 plants in total, 27 for each cultivar). These cultivars were selected based on dissimilarities in their development and yield potential resulting from previous field trials, which ultimately translate into different input requirements and adaptation to environmental challenges. Particularly, CB is a very-early cultivar (~52 days from planting to emerging silks) characterised by less vigorous and productive plants compared to the slow-growing (~71 days from planting to complete silk emergence), lush and high-yielding accessions of SF (USDA Agricultural Research Service U.S.D.O.A., 2015).

In this study, plants were sown in 54 2-L polyvinyl chloride (PVC) pots (180 mm diameter and 140 mm height) filled with a 70:30 mixture of sand and peat moss (~835 g) and 1 g $pot^{-1}$ of NPK Original Gold® slow-release nitrogen fertiliser (NPK 15-9-15; Compo GmbH® Münster, Germany). In order to avoid substrate and water losses, each pot was coated on the bottom with two breathable anti-leaching layers of tulle (~1.5 g) interspersed with water-absorbing expanded clay (~180 g). Seedlings were maintained for 28 days in a heated glasshouse under day/night temperature ≥15 °C and irrigated to soil saturation every two days. At 29 Days After Sowing (DAS) and for 45 days, plants were transferred to a cold glasshouse completely exposed to solar radiation and equipped with openable vents on the roof and walls for appropriate heating, humidity and air circulation. In this context, climatic conditions (i.e., relative humidity, air temperature and dew point) were automatically recorded and logged every 30 min using a Datalogger HOBO® Pro v2 (Onset Computer Corporation®, Bourne, MA, USA) weather station placed ~ 2 m above the canopies (Table S1). Plants were fully irrigated every other day and treated with 1 g $pot^{-1}$ of Greenleaf® nutrient solution (NPK 20-20-20; Biolchim®, Bologna, Italy) every 15 days until 46 DAS. Subsequently, each pot was sealed at the top in order to prevent evaporation from the soil surface, following Ferreira et al. (2015). In particular, the plant stem (diameter ≥10 mm) was enveloped with an expanded polyethylene (EPE foam) cylinder (75 mm diameter, 30 mm thickness and $3.50 \times 10^{-5}$ g $mm^{-3}$ density) at the substrate level, while a polyethylene film was adhered both to the pot and the EPE foam using one openable and one fixed PVC cable ties, respectively (Fig. S1). The weight of each sealed sample at field capacity (FCW) was measured after a full irrigation by allowing excess water to drain for 5 h.

At 46 DAS, two water treatments were imposed on the 54 maize plants by maintaining the 100% (T100; 15 plants x cultivar) and 25% (T25; 12 plants x cultivar) of the FCW (Table 3). The treatments were modulated for 28 consecutive days by using a 50 ml syringe body with 1 ml markings after weighing ($PW_{DAS}$) the individual pots every morning from 7:00 a.m. to 8:30 a.m.

### 2.4. Data collection and processing

#### 2.4.1. Microwave Sensing Experimental Setup

At 46 DAS, corresponding to plants with a stem diameter ≥10 mm, one spiral sensor was fixed just above the second internode of each of the 54 maize samples (Fig. 3a). The dielectric properties of a maize stem are usually maximised between the $2^{nd}$ and $3^{nd}$ internodes (excluding the lower stem section which in this experimentation could be affected by the pot seal), according to Sharma et al. (2020). The sensing measurements were performed from 46 to 74 DAS (Table S2) by connecting the probe loop to a calibrated N9918A 26.5 GHz FieldFox Vector Network Analyzer (Keysight Technologies®, Santa Rosa, CA, USA). Initially, the input impedance of the stand-alone probe was measured to test the efficient functioning of the probe loop, namely the effect of the ohmic losses incurred by the presence of the connector and the parasitic capacitance introduced by its soldering. Subsequently, the input impedance ($Z_{input}$) was acquired by positioning the probe loop close to each sensor applied on plants under both T100 and T25 treatments (Fig. 3b). The real and imaginary parts of the probe loop input impedance were recorded with 1001 frequency points on a linear scale over the frequency range 100–900 MHz. For each plant, three measures were averaged to avoid unreliable results and undesired oscillations.

Both the maximum of the real part ($\Re(Z_{input})$) and the resonance frequency $f_r$ shift of the probe loop input impedance were evaluated

**Table 2**
Water stress status from 1 (no stress) to 7 (stress) simulated dielectric properties.

| *Water stress status* | $\varepsilon'$ | $\sigma\ (Sm^{-1})$ |
|---|---|---|
| 1 | 60 | 1.5 |
| 2 | 50 | 1 |
| 3 | 40 | 0.8 |
| 4 | 30 | 0.6 |
| 5 | 20 | 0.4 |
| 6 | 15 | 0.2 |
| 7 | 10 | 0.1 |

**Table 3**
Average weight (± standard error) in grams (g) of "Cinquantino Bianchi" (CB) and "Scagliolo Frassine" (SF) maize samples maintained at 100% (T100) and 25% of FCW (T25; 15 and 12 samples per T100 and T25 treatments x cultivar, respectively) starting from 46 Days After Sowing (DAS).

| Cultivar | DAS | N° Samples | Average treatment weight (g) | |
|---|---|---|---|---|
| | | | $T100_{FCW}$ | $T25_{FCW}$ |
| *CB* | 46 | 27 | 1618.27 ± 20.29 | 1668.58 ± 16.96 |
| *SF* | 46 | 27 | 1625.33 ± 11.34 | 1643.58 ± 13.52 |

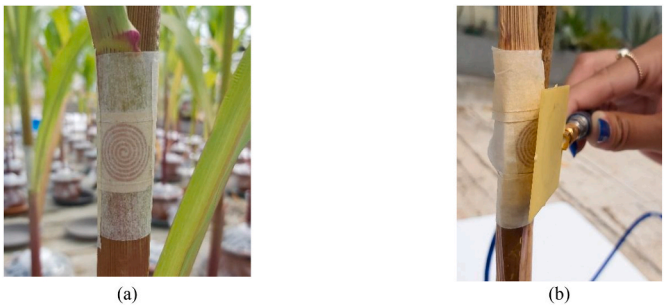

(a) (b)

**Fig. 3.** Experimental set-up: **(a)** the sensors were fixed with paper tape above the second internode of each of the 54 maize samples. **(b)** Method for acquiring the input impedance $Z_{input}$: the external probe loop, connected to a VNA, is positioned concentric and close to the sensor.

daily to detect the different trend over time between the two treatments for each cultivar.

### 2.4.2. Morpho-physiological measurements

Just after the microwave system measurements, the height (SH) and basal ($D_1$), half-plant ($D_2$) and apical diameters ($D_3$) of each stem were measured three times a week (between 46 and 74 DAS; Table S2) using a digital calliper (±1.0 mm accuracy) and combined in Eq. (9) for deriving the relevant stem volume (SV).

$$SV = \left\{ \left[ \pi + \left(\frac{D_1}{2}\right)^2 \left(\frac{SH}{3}\right) \right] + \left[ \pi + \left(\frac{D_2}{2}\right)^2 \left(\frac{SH}{3}\right) \right] + \left[ \pi + \left(\frac{D_3}{2}\right)^2 \left(\frac{SH}{3}\right) \right] \right\} \tag{9}$$

where the SV is approximated by summing up the volume of three superimposed cylinders of equal height $\left(\frac{SH}{3}\right)$ and variable radius $\left(\frac{D_n}{2}\right)$.

Subsequently, the minimum leaf water potential ($\Psi_{min}$) was collected on three randomly selected plants for each cultivar (*CB* and *SF*) and treatment (T100 and T25) between 12:00 p.m. and 14:00 p.m. (Table S2). The first leaf just above the sensor was cut at the base and for a couple of centimetres along the central vein with a cutter in order to insert it into the pressure chamber lid (PMS Instruments Co.®, Corvallis, OR, USA).

The fresh weight (FW) of individual sectioned organs (i.e., stem, leaves, inflorescences and ears) were then obtained using a precision balance (1000/0.001 g accuracy; Radwag®, Radom, Poland) and summed to derive the fresh above-ground biomass (FAGB). Meanwhile, root material was collected by washing off the soil and the fresh below-ground biomass (FBGB) was retrieved. The dry weight (DW) of stem, leaves, inflorescences, ears, above- (DAGB) and below-ground biomass (DBGB) was determined after oven drying the samples for 72 h at 70 °C. Then, the fresh (FWC; Eq. (10)) and dry base water content (DWC; Eq. (11)) were calculated for each accession, according to Zheng et al. (2015). Finally, the $\frac{DW_x}{FW_x}$ ratio was computed to retrieve the Percentage Dry Matter Content (PDMC; Eq. (12)) on the single organ basis, while the stem density ($\rho_{stem}$) was measured by relating its dry weight and volume (Eq. (13)).

$$FWC_x = \left[\frac{H_2O_x}{FW_x}\right] 100, \tag{10}$$

$$DWC_x = \left[\frac{H_2O_x}{DW_x}\right] 100, \tag{11}$$

$$PDMC_x = \left[\frac{DW_x}{FW_x}\right] 100, \tag{12}$$

$$\rho_{stem} = \left[\frac{DW_{stem}}{SV}\right], \tag{13}$$

where $x$ represents the analysed variable (i.e., stem, leaves, tassels, cobs, AGB or BGB) and $H_2O_x = (FW_x - DW_x)$ denotes the $x$ water content.

### 2.4.3. Anatomical and histochemical analysis

The part of the stem, with the sensor attached, was cut and preserved in ethyl alcohol, then frozen and cut with a microtome. The frozen sections were quickly transferred to a slide, stained for 5 s with safranin/Astra blue double staining, then washed with distilled water, dehydrated (50, 75 and 95 % ethanol) and examined with a light microscope (Nikon Eclipse 90i; Nikon, Tokio, Japan). The solution for dual safranin/Astra blue staining was prepared with 0.5 g of Astra blue powder in 100 ml of distilled water and 4 ml of acetic acid was added to the 1% aqueous safranin solution with the proportion 2:3. Staining with safranin/Astra blue allows recognition of lignification processes. Cell walls richer in lignin appear red, while those richer in cellulose are stained blue.

### 2.4.4. FTIR-ATR spectroscopy analysis

Attenuated total reflectance Fourier transform mid-infrared (ATR-FTIR) spectroscopy was performed on the external stem of three plants from each cultivar (CB and SF) at 46 DAS while maintaining 100% of the FCW (Field Capacity Water). Additionally, a single plant from each cultivar was analysed at 74 DAS under the two water treatments (100% FCW and 25% FCW). ATR-FTIR spectra were recorded using an Alpha FT-IR spectrometer (Bruker, Ettlingen, Germany). Each sample was scanned 40 times, with a resolution of 4 $cm^{-1}$, and the scanning range was set between 400 and 4000 $cm^{-1}$. The spectra were acquired directly from small samples of the external stem, without any specific pre-treatment, while still under waterlogged conditions. Water spectra were subtracted from the stem samples using specific software routines, and subsequent evaluations were carried out in the 700–1800 $cm^{-1}$ range of the subtracted spectra. Three replicated spectra were collected for every sample pressed on the ATR crystal. The acquired spectra were processed using OPUS 6.5 software by Bruker Optics.

### 2.4.5. Statistical analysis

Principal component analysis (PCA) was used to identify the morpho-physiological variables that most influence the sensor response. Moreover, the sensor performance was evaluated with Pearson's correlation coefficient ($r$) between the sensors' response and each of the analysed morpho-physiological variables. Finally, a $t$-test was used to examine the Percentage Dry Matter Content (PDMC), the variation of the maximum of the real part of the input impedance ($\max(\Re(Z_{input}))$) and the sensor's self-resonance frequency shift ($f_r$) between the two different water treatments. A $p$-value $\leq 0.05$ was considered significant. Linear regressions were also generated for each cultivar and treatment to predict the maximum of the real part of the input impedance ($\max(\Re(Z_{input}))$ from $FWC_{stem}$.

## 3. Results

### 3.1. Numerical-based sensor's response

Firstly, the input impedance of the stand-alone probe loop ($Z_{probe}$) was evaluated in the operative frequency range between 100 and 550 MHz (Fig. 4a). To take into account the parasitic capacitance resulting from the soldering process of the SMA connector to the driver, a capacitor C = 1.31 pF was inserted in parallel to the feeding port. Thus, the probe loop self-resonance frequency becomes 464 MHz instead of 1.67 GHz (which is the value of the ideal loop, without considering real scenario effects). The self-resonance of the probe loop was sufficiently far away from the sensor operative range, thus ensuring a purely inductive mutual coupling between them. Afterwards, the sensor

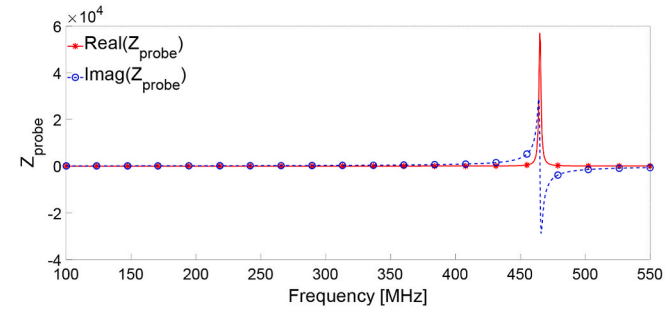


(a)

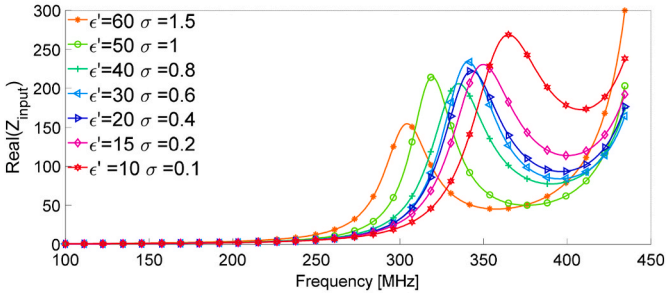


(b)

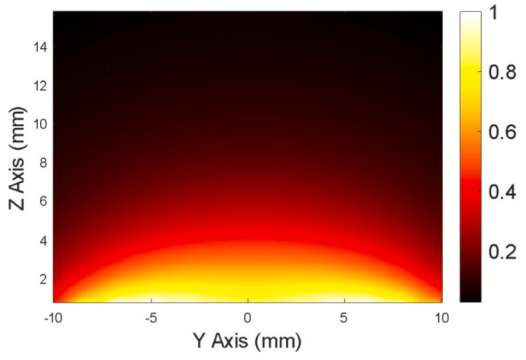


(c)

**Fig. 4.** Numerical results: **(a)** the real and imaginary part of the stand-alone probe loop impedance evaluated in the operative frequency range (100–550 MHz). Taking into account the parasitic capacitance at the feeding port, the stand-alone probe loop self-resonance is around 464 MHz; **(b)** variation of the real part of the input impedance ($\Re$ ($Z_{input}$)) for different water stress status; **(c)** normalised magnetic field map evaluated on a plane perpendicular to the stem (see Fig. 2c).

response to the increased water stress was investigated in order to correlate the health status of the maize plant to the probe loop input impedance. In this context, as the degree of water stress increased, a progressive linear increment of the maximum of the real part of the probe loop input impedance ($\Re$ ($Z_{input}$)) and of the resonance frequency ($f_r$) was observed (Fig. 4b). As previously reported, this behaviour results from water stress-induced dielectric characteristics variations that produce changes in the lumped spiral sensor equivalent circuit parameters (in particular $R_{eff}$ and $C_{eff}$). The observed percentage deviations in the real part of the input impedance amplitude and resonance frequency shift between stress states 1 (no stress) and 7 (maximum stress) was 20% and 73.7%, respectively.

In order to estimate the penetration depth into the maize stem, the normalised H-field map on a plane perpendicular to the sensor (zy plane in Fig. 4c) was calculated. The amplitude of the reactive magnetic field reached a depth of 8 mm with a normalised amplitude of 0.5.

### 3.2. Experimental sensor results

As reported in the Microwave Sensing Experimental Setup section, the input impedance of the stand-alone probe ($Z_{probe}$) was initially measured to analyse the effect of the ohmic losses caused by the connector and the parasitic capacitance introduced by its soldering. The experimental $Z_{loop}$ is reported in Fig. 5. As a general observation, an amplitude reduction can be observed with respect to the numerical set-up, while the parasitic capacitance introduced by the soldering agreed with simulations since the self-resonance frequency was around 460 MHz, as expected. The higher losses observed in measurements were mainly due to the fabrication process. PCB traces notoriously suffer from additional ohmic losses which are not considered in full wave simulations.

After this preliminary validation, Fig. 6 compares the spiral sensor 's response placed on CB and SF maize samples treated with T25 and T100, against time. In particular, in Fig. 6a-b, the variations of the real part of the input impedance peak (max($\Re$ ($Z_{input}$))) are reported. In Fig. 6c-d, the sensor's self-resonance frequency shifts ($f_r$) are depicted. According to the theoretical model, as the water stress increased day after day (blue full line), a resonant frequency upshift and an amplitude increment in the real component of the probe loop input impedance were observed for the CB maize cultivar. In contrast, the spiral sensor response of the maize plants of the T100 treatment (red dashed line) remained almost constant throughout the experiment, both in amplitude and in self-resonant frequency value, which was in agreement with the expectation. A significant difference between the two treatments can be observed in the variation of the maximum real part of $Z_{input}$ and $f_r$, respectively from 71 DAS and 70 DAS.

Regarding the spiral sensor applied to the SF maize cultivar, for both T25 and T100 treatments, as DAS increased there was a linear increase of max($\Re$ ($Z_{input}$)) and $f_r$ for both treatments but there was no statistical difference observed between the treatments.

### 3.3. Morpho-physiological, anatomical, and histochemical responses to water treatments

Consistent with the dielectric variations detected by the microwave sensor during the 28-day long monitoring, the total amount of transpired water was 53.27% (CB) and 62.41% (SF) lower in maize plants

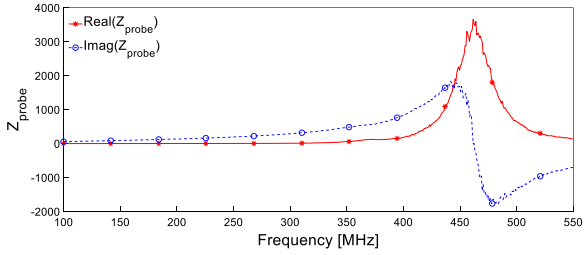


**Fig. 5.** Measured stand-alone probe loop impedance evaluated in the operative frequency range (100 MHz–550 MHz). The effect of the parasitic capacity due to the connector soldering is in excellent agreement with numerical simulations, with a self-resonance observed at 460 MHz.

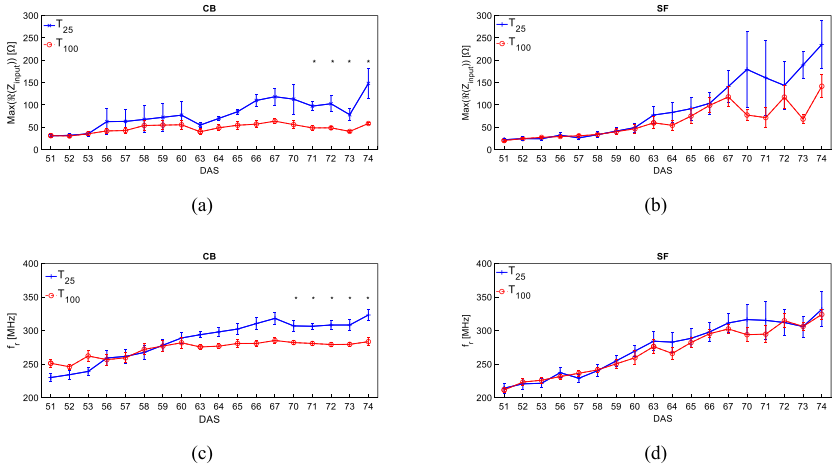


**Fig. 6.** Experimental results on: **(a)–(b)** variation of the maximum of the real input impedance of the system for treatments T25 (blue line) and T100 (red line), cultivar CB (left) and SF (right); **(c)–(d)** self-resonant frequency shift for treatments T25 (blue line) and T100 (red line), cultivar CB (left) and SF (right). Asterisks indicate significant statistical differences between plants under T25 and those under T100 according to *t*-test (*: $p \leq 0.05$). The vertical bars represent the standard error. (For interpretation of the references to colour in this figure legend, the reader is referred to the Web version of this article.)

subjected to the T25 treatment compared to the T100 condition (Fig. S2). In general, such differences increased gradually from ~50 DAS onwards ($p \leq 0.05$) and reached the maximum peak at ~ 60 DAS (CB.; 192.27 g, on average) and ~74 DAS (SF.; 292.50 g, on average). The trend of rising transpiration rates recorded for fully irrigated CB plants stabilised after the earlier developmental stages and partially decreased from ~61 DAS, which resulted in non-significant differences with respect to the T25 samples at 74 DAS. Particularly, the deficit-irrigated CB plants maintained an almost constant water loss from ~51 DAS until the end of the experiment (ranging from 94.00 to 145.46 g, on average), as highlighted by the 50.43% higher variance detected in the T100 plants for the same period. Contrariwise, the transpiration rate of the full-irrigated SF plants rose in a roughly linear fashion, reaching average values during the last 4 monitoring days of 4.91–5.67 that were 3.55–4.28 times greater than the baseline (i.e. 46 DAS) and the T25 conditions ($p \leq 0.05$), respectively. Although remaining significantly lower compared to the full-irrigation throughout the experiment ($p \leq 0.05$; 60.93% lower values, on average), the water loss by SF plants under T25 slightly increased up to ~ 60 DAS (109.60 g, on average) and then decreased with a linear-like pattern (92.61 g, on average), which was similar to the CB samples subjected to the same treatment.

Despite the observed variability in transpiration rates, deficit-irrigation did not significantly affect the above-ground Percentage Dry Matter Content (PDMC) of both cultivars (Fig. S3). At the whole-plant scale, the PDMC showed a progressive increase up to 15.34% and 11.73% (under T100 and T25, respectively) in CB and up to 15.22% and 5.84% (under T100 and T25, respectively) in SF as the maturation phase progressed. The differences between treatments were almost always non-significant ($p > 0.05$) regardless of the plants' age. For both cultivars, the leaves' PDMC slightly increased with water deficit reaching an exacerbated deviation from T100 only for CB at 67 DAS ($p \leq 0.05$; 21.72% higher values, on average). In contrast, the stem, ear and cob (maturity stage reached only by the early CB) dry matter in plants under T25 was respectively on average 16.22%, 25.96% and 13.07% lower than in the full-irrigation treatment (T100) starting from 60 (CB) and 67 DAS (SF). The PDMC in the stems and ears was always higher in CB at advanced maturity stages for both the treatments during the experiment.

Focusing on the maize stem density (Fig. S4), only the CB plants showed a significant reduction at the end of the water shortage period ($p \leq 0.05$; 30.91% lower values compared to T100 samples, on average). In particular, the average $\rho_{stem}$ under T25 increased by up to 25.91% from 46 to 68 DAS, albeit at a lower rate compared to the control plants (30.51% increase, on average). After this date, the stem density under T25 abruptly decreased (9.30% lower values at 74 DAS, on average), while the T100 values continued to rise until the end of monitoring (18.78% higher values at 74 DAS, on average). Conversely, the $\rho_{stem}$ in SF samples under deficit-irrigation reached similar levels to those of the control plants throughout the experiment, by slightly deviating from the baseline range (i.e., 46 DAS).

The stem sections of the CB submitted to the safranin/Astra blue staining showed very slight pink staining in the outer part of the stem, at 46 DAS and 74 DAS in the T100 treatment only (Fig. S5 A and B). In the T25 treatment, no pink stained cells were evident, while there was a conspicuous increase in sclerenchymatous cells around the bundles. In the outer leaves enveloping the stem, the sclerenchymatous cells reached up to the epidermis, creating zones of thickening (Fig. S5 C arrow), while in the stem they created a continuous zone below the epidermis (Fig. S5 D arrow). Similar to the CB results, cells with very slight positive staining to safranin/Astra blue dye were evident at both 46 DAS and 74 DAS for SF under T100 and T25 treatments in the outer part of the stem. The anatomical structure of the T100 and T25 samples also did not appear to undergo any major changes other than a slight thickening of the cell layers under the epidermis (Fig. S5 E, F and G).

The spectral profiles of the external stem sections in the analysed samples from the two maize cultivars, CB and SF, can be observed in Figs. S6a and S6b, respectively. It was observed that the general spectral profile in the range of 1800-700 $cm^{-1}$ was similar, but certain characteristic bands exhibited changes in absorbance and/or wavenumber. For selected bands in the FTIR spectra, the relative absorption values are provided in terms of a specific lignin band at 1505 $cm^{-1}$, corresponding to the C=C aromatic skeletal vibrations stretching of the benzene ring in lignin. Regarding the maize cultivar CB, a low detectable amount of lignin was found for three plants at 46 DAS with 100% of the FCW. However, in the case of one CB sample, lignin was not detectable through spectroscopy. Both plants analysed at 74 DAS under two water treatments, 100% and 25%, exhibited a quantity of lignin that was not extremely high but still comparable and slightly higher than the stems analysed at 46 DAS (Fig. S6a). For the maize cultivar SF, the presence of lignin is noticeable both at 46 DAS (except for one SF sample, possibly due to the selection of the upper portion of the plant during sampling) and at 74 DAS under the T100 and T25 treatments in the outer section of the stem. However, at 46 DAS, the amount of lignin did not seem comparable between sample S1 and S3, with the latter showing lower quantities. Additionally, under the T25 water stress condition, the

quantity of lignin appeared to be significantly reduced compared to the T100 treatment (Fig. S5b).

### 3.4. Modelling relationship between morpho-physiological parameters and sensor response to water treatments

The principal component analysis (PCA) on the whole dataset provided a two-dimensional pattern (Fig. 7), explaining 60% of the total variance. PCA revealed good discrimination between the CB maize cultivar under treatment T25 and CB and SF maize cultivar under treatment T100 and T25. Sensor parameters ($f_r$ and max($\Re$ $(Z_{input})$)) had the highest inverse correlation with morphological parameters $DWC_{AGB}$ and $FWC_{AGB}$ (Figs. S7 and S8 and Table S3) afferent to the aerial part (stem, leaves, ear and cob). Since the sensor is fixed directly on the stem (fraction of the aerial component), the correlation between the content of $FWC_{stem}$ (%) and the sensor variables $f_r$ and max($\Re$ $(Z_{input})$) were evaluated individually. In particular, data analysis showed a higher correlation between $f_r$ , max($\Re$ $(Z_{input})$) and $FWC_{stem}$.

Regarding CB (Figs. S9a and b)), from ∿ 67 DAS it becomes evident that a discernible discrepancy between the T25 (red symbols) and T100 curves (blue symbols) can be detected. With a reduced water supply, the max($\Re$ $(Z_{input})$) and $f_r$ increased and an inverse linear correlation coefficient between the two variables was observed (Table 4). In contrast, the max($\Re(Z_{input})$) and $f_r$ of the sensors applied to the CB maize species under T100 remained almost constant in a range between 17 and 52 Ohm and 250–300 MHz with a correlation coefficient r equal to −0.78 and −0.64. Regarding the SF cultivars (Figs. S9c and d)), for both treatments T25 and T100 a linear increase of max($\Re$ $(Z_{input})$) and $f_r$ was observed as water supply decreased. Regression analysis parameters are reported in Table 4.

## 4. Discussion

In this paper, an innovative microwave sensor has been presented for real time, non-destructive monitoring of plant's water stress status. Its

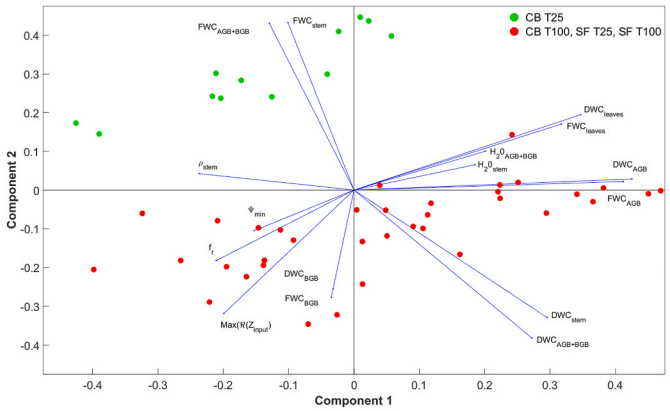


**Fig. 7.** Graphical representation of the principal component analysis conducted on the analysed parameters: $FWC_{AGB+BGB}$ = above + below ground biomass fresh base water content; $FWC_{AGB}$ = above ground biomass fresh base water content; $FWC_{BGB}$ = below ground biomass fresh base water content; $FWC_{stem}$ = stem fresh base water content; $FWC_{leaves}$ = leaves fresh base water content; $DWC_{AGB+BGB}$ = above + below ground biomass dry base water content; $DWC_{AGB}$ = = above ground biomass dry base water content; $DWC_{BGB}$ = = below ground biomass dry base water content; $DWC_{stem}$ = = stem dry base water content; $DWC_{leaves}$ = leaves dry base water content; $H_2O_{AGB+BGB}$ = above + below ground biomass water content; $H_2O_{stem}$ = stem water content; ρstem = stem density; $\Psi_{min}$ = minimum leaf water potential; $f_r$ = resonant frequency; max($\Re$ $(Z_{input})$) = maximum of the real part of the input impedance. The blue lines represent all variables that contribute to discriminating between treatments. (For interpretation of the references to colour in this figure legend, the reader is referred to the Web version of this article.)

**Table 4**
Correlation and regression analysis summary for the relationship between spiral sensor parameters (max ($\Re$ $(Z_{input})$), $f_r$) and $FWC_{stem}$ across different cultivars (CB, SF) and treatments (T25, T100).

| Cultivar | Treatment | Equation | r |
|---|---|---|---|
| CB | T25 | max ($\Re$ ($Z_{input}$)) = −18.41 $FWC_{stem}$ +1652.32 | −0.89 |
| | T100 | max ($\Re$ ($Z_{input}$)) = −3.211 $FWC_{stem}$ +316.72 | −0.83 |
| SF | T25 | max ($\Re$ ($Z_{input}$)) = −35.87 $FWC_{stem}$ +3230.46 | −0.70 |
| | T100 | max ($\Re$ ($Z_{input}$)) = −11.94 $FWC_{stem}$ +1118.64 | −0.83 |
| CB | T25 | $f_r$ = −10.54 $FWC_{stem}$ +1186.16 | −0.78 |
| | T100 | $f_r$ = −2.92 $FWC_{stem}$ +514.29 | −0.64 |
| SF | T25 | $f_r$ = −17.72 $FWC_{stem}$ +1821.74 | −0.60 |
| | T100 | $f_r$ = −8.92 $FWC_{stem}$ +1052.7 | −0.81 |

proven capacity to accurately identify the morpho-physiological variations at the organ and whole plant level represents an instrumental step towards the improved comprehension of genetic mechanisms underlying crop responses in resource-limited environments. Accordingly, the sensor is a promising tool for breeding more resilient cultivars to water scarcity, as well as for the optimised management of irrigation strategies.

The strength of the implemented microwave sensor can be ascribed to its remarkable technical characteristics and cost-effectiveness. In particular, this wireless technology eliminates the need for a physical microchip, thus making it a cost-effective alternative when juxtaposed with chip-based RFID systems, as documented by Costa et al. (2021), and commercially available instruments, such as TDR and leaf sensors, as highlighted in the works of Majcher et al. (2020), *AgriHouse Inc. (2017)* and Decagon Devices Inc (2016). The sensor's distinctive capability to actively oversee the physiological well-being of living plants was achieved through direct interfacing. Firstly, this was enabled by the chosen flexible, compact, and non-invasive configuration, which was amenable to adaptation for all plant organs, exemplified here by its application to the stem (Wang et al., 2018). Secondly, the sensor's capacity for real-time monitoring of dielectric property variations in the stem accommodated the detection of specific and precise physiological changes. This level of accuracy overcomes that of soil sensors, which predominantly focus on moisture level measurements, providing only indirect insights into plant health (Cappelli et al., 2021; Daskalakis et al., 2016). Similarly, leaf sensors furnish indirect assessments of a plant's health status, often derived from detached leaf specimens, as explored by Dey et al. (2020) and Yan et al. (2020), or predicated on temperature differentials between leaves and the ambient air, as expounded upon by Palazzi, Bonafoni, et al. (2019a). Moreover, it is crucial to underline the environmental friendliness and non-intrusiveness of this sensor within its natural habitat deployment. Specifically, the non-invasive attributes of the proposed sensor guarantees the overall health of the plant, reducing the risk of inducing stress or infection, in stark contrast to other *in vivo* solutions that necessitate the insertion of steel needles into the stem to measure electric impedance variations (Comparini et al., 2020; Garlando et al., 2022). Lastly, according to the literature, numerous investigations have been undertaken to assess the influence of different geometric factors, including diameter, spacing between turns and number of turns, on the operational efficacy of the resonator (Sarhadi et al., 2013; Sergienko et al., 2016; Virdee and Grassopoulos, 2003). These studies have demonstrated that the maximisation of the Q-factor throughout the design phase resulted in a discernible enhancement in system sensitivity and resolution. Consequently, the Q-factor optimization procedure described in the design process provided a substantial contribution towards achieving optimal performance.

As research progresses into the complex processes by which crops react to environmental stressors, including drought, it becomes apparent that understanding their physiological adaptations is of paramount importance. Indeed, signal transduction pathways activate plant adaptive responses, encompassing physiological and molecular adjustments (Nawaz et al., 2023). These responses, in turn, lead to shifts in resource

allocation patterns and consequential alterations in the growth dynamics of individual organs. The complex interaction described above sets the stage for the water status monitoring of two maize cultivars (CB and SF) subjected to different irrigation treatments (T100 and T25) for a duration of 17 days. The objective was to establish a correlation between the sensor response (i.e., $\max(\Re(Z_{input}))$ and $f_r$) and pertinent morpho-physiological parameters to evaluate the potential application of the implemented sensor in detecting plant water status. Indeed, the variations in the electrical signal recorded over time on vegetative organs (e.g, leaves) have been successfully related to hydration deficits, albeit with approaches that could impair the physiology of living plants (Garlando et al., 2022). Self-adhering surface microelectrodes have been recently developed for measuring leaves' electrophysiology, avoiding damage to plants with directly implanted contacts (Meder et al., 2021). Nevertheless, leaf wearable sensors can interfere with plant growth by hindering gas exchange and reducing light absorption, which restricts their applicability for detecting the occurrence of morpho-physiological adaptations triggered by water stress (Zhang et al., 2023). The lightweight, soft, and bendable configuration of the proposed microwave sensor guarantees a non-invasive monitoring of the single-plant water status through an in-depth evaluation of stem dielectric properties oscillations under drying conditions. Specifically, the constant trend of the signal recorded on fully irrigated plants (T100) differed from the sensor response of the samples subjected to T25 treatment, which were characterised by an overall upshift of $f_r$ and a rising of $\max(\Re(Z_{input}))$ (Fig. 6). As a matter of fact, progressive increases in the stem signal variance can be generally associated with the occurrence of plant responses to water stress (Lazzoni et al., 2022; Sharma et al., 2020). This assumption is supported in this study by the lower transpiration rate experienced under limited irrigation conditions that reflected a typical stress-related effect of stomata closure on photosynthetic activity (Flexas et al., 2004). Such an adaptive pathway may be associated with the diminished AGB accumulation and partitioning, which negatively impacted the stem Percentage Dry Matter Content (PDMC) at advanced development stages. In line with these findings, previous studies have demonstrated how the maize stem is more sensitive to water stress than other above-ground organs (e.g., leaves and silks) involved in the quick mobilisation of reserve assimilates to reproductive organs (Ma et al., 2018; Westgate and Boyer, 1985; Yousaf et al., 2023). This evidence confirms that the signal propagation of this sensor responds to changes in the structural and hydraulic composition of maize stem induced by different irrigation treatments.

Anatomical adjustments of maize stem against water stress vary significantly depending on the varietal characteristics and its growth period, underlying biochemical and histological adaptations that could contribute to the electric signal variability (El Hage et al., 2021; Kränzlein et al., 2022; Nadler et al., 2008). The responses of the proposed sensor showed how the tested maize cultivars behaved differently in balancing the stem's moisture and dry matter based on the phenological stage and stress condition. In particular, very-early CB plants experienced drought between reproduction and grain filling time (Fig. S2), which has been recognized as the most critical among all stages of maize growth (Singh et al., 2023). This led to a significant decrease in the stem density ($\rho_{stem}$) at advanced maturity compared to fully irrigated plants, with consequently higher dielectric responses registered toward the end of the experimentation. Such a depletion was mainly attributable to the observed absence of lignified tissues in stressed CB plants, which was justified by the counterproductive nature of synthesising hydrophobic molecules under water-depleted conditions (El Hage et al., 2018, 2021; Stubbs et al., 2022). To compensate, a notable enlargement of sclerenchymatous cell layers surrounding the epidermis-reaching beams conferred greater mechanical strength to vascular tissue by minimising water loss (Fig. S5),which has as already been observed for wheat (Waseem et al., 2021), rice (Mostajeran and Rahimi-Eic, 2008) and other plant species (Nawazish et al., 2006). Indeed, stem cross-sectional thickness promotes the formation of storage parenchyma, enabling the plant to maintain water potential under prolonged drought periods (Plavcová and Jansen, 2015; Waseem et al., 2021). In this study, this guaranteed a percentage hydration of the stem ($FWC_{stem}$) under T25 almost equal to the T100 treatment, although an immediate reduction in transpiration was observed as a typical isohydric maize behaviour (Tardieu and Simonneau, 1998). Thus, sclerification endowed stressed plants with different dielectric properties compared to fully irrigated plants that showed a constant sensing response attributable to the absence of significant tissue changes except for an exiguous synthesis of lignin and a consequent increase of $\max(\Re(Z_{input}))$ and $f_r$ at maturity stages. On the other hand, no significant variations in the development of morpho-physiological traits, including $\rho_{stem}$, were detected for the slow-growing SF cultivar that had to deal with deficit irrigation during vegetative and early flowering phases (Fig. 7 and Fig. S3). As a matter of fact, maize was relatively insensitive to water stress imposed before kernel development because of the relatively lower water requirements (Mansouri-Far et al., 2010). Nevertheless, the generalised frequency shift and amplitude variation detected by the sensor throughout the experiment could be attributed to the incremental presence of lignified tissues within the outer section of the stem (i.e., rind). In line with these findings, it has been previously demonstrated that maize plants subjected to water stress could synthesise less lignin compared to optimal conditions and preferentially accumulate it inside the rind rather than in deeper parenchymal tissues (El Hage et al., 2018; Legland et al., 2017). Such an adaptive mechanism may explain the divergence in the signal detected between stressed and non-stressed SF plants, confirming the sensitivity of the proposed sensor also to slight changes in the biochemical composition of plant tissues due to water treatments. The sensor's ability to detect variations in both water content and histology is a notable advantage in assessing stress levels. However, it may also be a limitation as it can be difficult to understand if such variations are due to stress or plant growth.

To overcome this constraint, an effective solution could be a further implementation of the presented sensor with a dual-layer architecture in order to increase the sensitivity (Brizi et al., 2020). The objective of this strategy is to enhance the magnetic field through the use of a two-layer spiral resonator, with one layer exhibiting "left-handed" characteristics and the other layer exhibiting "right-handed" characteristics, both of which are interconnected at their own ends. In this manner, a continuous configuration is achieved, facilitating the unidirectional flow of electric current and, thus, amplifying the magnetic field. Furthermore, it is important to address the impact of temperature variations on the dielectric properties of water and plant tissues, as highlighted in the literature (Seyfried & Grant, 2007; Ulaby and El-rayes, 1987; Ulaby and Jedlicka, 1984). Indeed, the temperature dependence can affect the sensor's readings and lead to wrong conclusions on the plant health status. A solution to mitigating this issue consists in an accurate calibration to be conducted under different temperature conditions. Establishing the baseline for the sensor output at various temperatures will allow for corrections to be implemented during actual field measurements. In this experiment, measurements were specifically conducted at the same time each day to ensure consistent temperature conditions, thereby minimising variability in the data. To better assess the sensitivity of the sensor, additional factors that can be modified include the placement of the sensor on the plant in regions or organs that are more susceptible to water scarcity, as well as the selection of different crop species characterised by slower growth rates, such as tree crops. Moreover, being a prototype, the sensor is not suitable for crop monitoring in an open field because meteorological phenomena, such as precipitation or intense wind could damage it and detach it from the plant stem. Therefore, future developments should be directed at enhancing the sensor's mechanical robustness and environmental resilience. These improvements should include the development of suitable protective structures and anchoring systems to ensure the sensor's operational stability and mechanical integrity, even under adverse weather conditions. Additionally, the use of a Vector Network Analyzer (VNA) for

sending and collecting the RF signal is currently recognized as a limitation due to its impracticality for field deployment. In the implementation phase, each reading VNA should be replaced with a handheld device or even with an integrated circuit connected with the other in a mesh network supported by IoT communication technologies. Such a transition should make the measuring system more practical for real-time crop monitoring beyond the prototype stage. In summary, while the methodology for monitoring plant water status was effective, enhancing the hardware is essential for broader application. With these improvements, the sensor could be used for more optimised and sustainable water resource management, particularly in the context of precision agriculture and climate change adaptation.

## 5. Conclusion

In this paper, an innovative sensing configuration has been presented for non-destructively assessing the water status of plants. This configuration employs a self-resonant spiral coil, which is sensitive to the target composition variation, and inductively coupled to a probe loop. The latter has the dual purpose of supplying power and reading the output signal. The equivalent RLC circuit model was used to analytically describe the sensor's operating principle and the design was achieved following a Q-factor optimization procedure to maximise the system sensitivity. The sensor performance has been evaluated numerically and experimentally to demonstrate the relations among the maximum of the real part of the input impedance, the resonance frequency and plant's health status. In particular, the water stress monitoring was achieved by recording the system parameters variations which are dependent on the stem dielectric properties. Specifically, the spectral profiles of the external stem sections and the correlation between the content of $FWC_{stem}$ (%) and the sensor variables $f_r$ and $\max(\Re\ (Z_{input}))$ helped in distinguishing the overall behaviour of two maize cultivars to deficit water treatments. The proven sensor's capacity to detect morphological and histological alterations may limit other practical applications, as discerning whether these modifications are attributable to stress responses or plant growth is challenging. For this reason, future developments will be devoted to strengthening the sensor magnetic field to enhance the sensor performance and modelling the structure of the stem in order to find the parameters of the individual tissues for a more thorough test of the sensitivity of the sensor. Finally, while the sensor demonstrates a significant potential, its application for widespread irrigation control requires further refinement, particularly in making the sensor more robust and resilient in field conditions. If these challenges are overcome, the enhanced sensor could facilitate more optimised and sustainable management of water resources, enabling efficient irrigation practices tailored to the real-time needs of plants and crops.

## Funding

This research did not receive any specific grant from funding agencies in the public, commercial, or not-for-profit sectors.

## CRediT authorship contribution statement

**Valeria Lazzoni:** Writing – original draft, Software, Investigation, Formal analysis, Conceptualization. **Danilo Brizi:** Writing – review & editing, Supervision, Methodology, Conceptualization. **Nicolina Staglianò:** Investigation. **Cristiana Giordano:** Writing – original draft, Methodology, Investigation. **Elisa Pecoraro:** Writing – original draft, Investigation. **Monica Anichini:** Investigation. **Francesca Ugolini:** Writing – original draft, Investigation. **Marco Bindi:** Supervision, Resources, Conceptualization. **Giovanni Argenti:** Supervision. **Agostino Monorchio:** Supervision, Resources, Conceptualization. **Riccardo Rossi:** Writing – original draft, Software, Methodology, Investigation, Formal analysis, Conceptualization.

## Declaration of competing interest

The authors declare that they have no known competing financial interests or personal relationships that could have appeared to influence the work reported in this paper.

## Appendix A. Supplementary data

Supplementary data to this article can be found online at https://doi.org/10.1016/j.biosystemseng.2024.08.007.

## References

Adelakun, I. A., & Sri Ranjan, R. (2013). Design of a multilevel TDR probe for measuring soil water content at different depths. *Transactions of the American Society of Agricultural and Biological Engineers, 56*, 1451–1460. https://doi.org/10.13031/trans.56.100109

AgriHouse Inc. (2017). SG-1000 leaf sensor [Online]. Available: https://www.biocontrols.com/Leaf/20Sensor/SG-1000softwareV1.pdf.

Boada, M., Lazaro, A., Villarino, R., Gil, E., & Girbau, D. (2018). Near-field soil moisture sensor with energy harvesting capability. In *2018 48th European microwave conference (EuMC)* (pp. 235–238). IEEE. https://doi.org/10.23919/EuMC.2018.8541569.

Brizi, D., Fontana, N., Costa, F., & Monorchio, A. (2019). Accurate extraction of equivalent circuit parameters of spiral resonators for the design of metamaterials. *IEEE Transactions on Microwave Theory and Techniques, 67*, 626–633. https://doi.org/10.1109/TMTT.2018.2883036

Brizi, D., Stang, J. P., Monorchio, A., & Lazzi, G. (2020). A compact magnetically dispersive surface for low-frequency wireless power transfer applications. *IEEE Transactions on Antennas and Propagation, 68*, 1887–1895. https://doi.org/10.1109/TAP.2020.2967320

Brocca, L., Tarpanelli, A., Filippucci, P., Dorigo, W., Zaussinger, F., Gruber, A., & Fernández-Prieto, D. (2018). How much water is used for irrigation? A new approach exploiting coarse resolution satellite soil moisture products. *Int. J. Appl. Earth Obs. Geoinformation, 73*, 752–766. https://doi.org/10.1016/j.jag.2018.08.023

Cappelli, I., Fort, A., Mugnaini, M., Panzardi, E., Pozzebon, A., Tani, M., & Vignoli, V. (2021). Battery-less HF RFID sensor tag for soil moisture measurements. *IEEE Transactions on Instrumentation and Measurement, 70*. https://doi.org/10.1109/TIM.2020.3036061

Chan, Y. J., Carr, A. R., Roy, S., Washburn, C. M., Neihart, N. M., & Reuel, N. F. (2022). Positionally-independent and extended read range resonant sensors applied to deep soil moisture monitoring. *Sens. Actuators Phys., 333*. https://doi.org/10.1016/j.sna.2021.113227

Cheng, X., Yan, X., Grantz, D. A., Xiang, Y., De Oliveira, R. F., Huang, L., Wang, Z., Du, T., & Cheng, Q. (2021). In-situ and non-invasive measurement of stem water content of trees using an innovative interdigitated-electrodes dielectric sensor less susceptible to stem diameter variation. *Agricultural and Forest Meteorology, 307*, Article 108473. https://doi.org/10.1016/j.agrformet.2021.108473

Comparini, D., Masi, E., Pandolfi, C., Sabbatini, L., Dolfi, M., Morosi, S., & Mancuso, S. (2020). Stem electrical properties associated with water stress conditions in olive tree. *Agricultural Water Management, 234*. https://doi.org/10.1016/j.agwat.2020.106109

Costa, F., Brizi, D., Genovesi, S., Monorchio, A., Manara, G., Requena, F., & Perret, E. (2019). Wireless detection of water level by using spiral resonators operating in sub-GHz range. In *2019 IEEE int. Conf. RFID technol. Appl. RFID-TA 2019* (pp. 197–200). https://doi.org/10.1109/RFID-TA.2019.8892141

Costa, F., Genovesi, S., Borgese, M., Michel, A., Dicandia, F. A., & Manara, G. (2021). A review of rfid sensors, the new frontier of internet of things. *Sensors, 21*. https://doi.org/10.3390/s21093138

da Fonseca, N. S. S. M., Freire, R. C. S., Batista, A., Fontgalland, G., & Tedjini, S. (2017). A passive capacitive soil moisture and environment temperature UHF RFID based sensor for low cost agricultural applications. In *2017 SBMO/IEEE MTT-S international microwave and optoelectronics conference (IMOC)* (pp. 1–4). IEEE. https://doi.org/10.1109/IMOC.2017.8121099.

Dadshani, S., Kurakin, A., Amanov, S., Hein, B., Rongen, H., Cranstone, S., Blievernicht, U., Menzel, E., Léon, J., Klein, N., & Ballvora, A. (2015). Non-invasive assessment of leaf water status using a dual-mode microwave resonator. *Plant Methods, 11*, 1–10. https://doi.org/10.1186/s13007-015-0054-x

Daskalakis, S. N., Assimonis, S. D., Kampianakis, E., & Bletsas, A. (2016). Soil moisture scatter radio networking with low power. *IEEE Transactions on Microwave Theory and Techniques, 64*, 2338–2346. https://doi.org/10.1109/TMTT.2016.2572677

Daskalakis, S. N., Goussetis, G., Assimonis, S. D., Tentzeris, M. M., & Georgiadis, A. (2018). A uW backscatter-morse-leaf sensor for low-power agricultural wireless sensor networks. *IEEE Sensors Journal, 18*, 7889–7898. https://doi.org/10.1109/JSEN.2018.2861431

Decagon Devices, Inc. (2016). PHYTOS 31, dielectric leaf wetness sensor, product manual [Online]. Available: http://library.metergroup.com/Manuals/10386_Leaf/20Wetness/20Sensor_Web.pdf.

Deng, F., Zuo, P., Wen, K., & Wu, X. (2020). Novel soil environment monitoring system based on RFID sensor and LoRa. *Computers and Electronics in Agriculture, 169*. https://doi.org/10.1016/j.compag.2019.105169

Dey, S., Amin, E. M., & Karmakar, N. C. (2020). Paper based chipless RFID leaf wetness detector for plant health monitoring. *IEEE Access, 8*, 191986–191996. https://doi.org/10.1109/ACCESS.2020.3033191

El Hage, F., Legland, D., Borrega, N., Jacquemot, M.-P., Griveau, Y., Coursol, S., Méchin, V., & Reymond, M. (2018). Tissue lignification, cell wall *p* -coumaroylation and degradability of maize stems depend on water status. *Journal of Agricultural and Food Chemistry, 66*, 4800–4808. https://doi.org/10.1021/acs.jafc.7b05755

El Hage, F., Virlouvet, L., Lopez-Marnet, P.-L., Griveau, Y., Jacquemot, M.-P., Coursol, S., Méchin, V., & Reymond, M. (2021). Responses of maize internode to water deficit are different at the biochemical and histological levels. *Frontiers of Plant Science, 12*, Article 628960. https://doi.org/10.3389/fpls.2021.628960

Eroglu, O., Kurum, M., & Ball, J. (2019). Response of GNSS-R on dynamic vegetated terrain conditions. *Ieee Journal of Selected Topics in Applied Earth Observations and Remote Sensing, 12*, 1599–1611. https://doi.org/10.1109/JSTARS.2019.2910565

Ferreira, L. C., Neiverth, W., Maronezzi, L. F. F., Sibaldelli, R. N. R., Nepomuceno, A. L., Farias, J. R. B., & Neumaier, N. (2015). Efficiency of cover materials in preventing evaporation in drought-stressed soybeans grown in pots. *Rev. Ciênc. Agrar. - Amaz. J. Agric. Environ. Sci., 58*, 349–356. https://doi.org/10.4322/rca.1861

Flexas, J., Bota, J., Cifre, J., Mariano Escalona, J., Galmes, J., Gulias, J., Lefi, E.-K., Florinda Martinez-Canellas, S., Teresa Moreno, M., Ribas-Carbo, M., Riera, D., Sampol, B., & Medrano, H. (2004). Understanding down-regulation of photosynthesis under water stress: Future prospects and searching for physiological tools for irrigation management. *Annals of Applied Biology, 144*, 273–283. https://doi.org/10.1111/j.1744-7348.2004.tb00343.x

Garlando, U., Calvo, S., Barezzi, M., Sanginario, A., Motto Ros, P., & Demarchi, D. (2022). Ask the plants directly: Understanding plant needs using electrical impedance measurements. *Computers and Electronics in Agriculture, 193*, Article 106707. https://doi.org/10.1016/j.compag.2022.106707

Gopalakrishnan, S., Waimin, J., Raghunathan, N., Bagchi, S., Shakouri, A., & Rahimi, R. (2021). Battery-less wireless chipless sensor tag for subsoil moisture monitoring. *IEEE Sensors Journal, 21*, 6071–6082. https://doi.org/10.1109/JSEN.2020.3039363

Gopalakrishnan, S., Waimin, J., Zareei, A., Sedaghat, S., Raghunathan, N., Shakouri, A., & Rahimi, R. (2022). A biodegradable chipless sensor for wireless subsoil health monitoring. *Scientific Reports, 12*. https://doi.org/10.1038/s41598-022-12162-z

Hardie, M. (2020). Review of novel and emerging proximal soil moisture sensors for use in agriculture. *Sens. Switz., 20*, 1–23. https://doi.org/10.3390/s20236934

Hornero, G., Gaitán-Pitre, J. E., Serrano-Finetti, E., Casas, O., & Pallas-Areny, R. (2017). A novel low-cost smart leaf wetness sensor. *Computers and Electronics in Agriculture, 143*, 286–292. https://doi.org/10.1016/j.compag.2017.11.001

Intergovernmental Panel On Climate Change (Ipcc). (2023). *Climate change 2022 – impacts, adaptation and vulnerability: Working group II contribution to the sixth assessment report of the intergovernmental Panel on climate change* (1st ed.). Cambridge University Press. https://doi.org/10.1017/9781009325844

Janni, M., Coppede, N., Bettelli, M., Briglia, N., Petrozza, A., Summerer, S., Vurro, F., Danzi, D., Cellini, F., Marmiroli, N., Pignone, D., Iannotta, S., & Zappettini, A. (2019). In vivo phenotyping for the early detection of drought stress in tomato. *Plant phenomics 2019*. https://doi.org/10.34133/2019/6168209

Kränzlein, M., Geilfus, C.-M., Franzisky, B. L., Zhang, X., Wimmer, M. A., & Zörb, C. (2022). Physiological responses of contrasting maize (Zea mays L.) hybrids to repeated drought. *Journal of Plant Growth Regulation, 41*, 2708–2718. https://doi.org/10.1007/s00344-021-10468-2

Kulundžić, A. M., Vuletić, M. V., Kočar, M. M., Mijić, A., Varga, I., Sudarić, A., Cesar, V., & Lepeduš, H. (2021). The combination of increased temperatures and high irradiation causes changes in photosynthetic efficiency. *Plants, 10*. https://doi.org/10.3390/plants10102076

Lazzoni, V., Canicatti, E., Brizi, D., Rossi, R., Moriondo, M., Bindi, M., & Monorchio, A. (2022). Non-destructive olive tree dielectric properties characterization by using an open-ended coaxial probe. In *2022 IEEE international symposium on antennas and propagation and USNC-ursi radio science meeting (AP-S/URSI)* (pp. 1412–1413). IEEE. https://doi.org/10.1109/AP-S/USNC-URSI47032.2022.9886505.

Legland, D., El-Hage, F., Méchin, V., & Reymond, M. (2017). Histological quantification of maize stem sections from FASGA-stained images. *Plant Methods, 13*, 84. https://doi.org/10.1186/s13007-017-0225-z

Ma, X., He, Q., & Zhou, G. (2018). Sequence of changes in maize responding to soil water deficit and related critical thresholds. *Frontiers of Plant Science, 9*, 511. https://doi.org/10.3389/fpls.2018.00511

Majcher, J., Kafarski, M., Wilczek, A., Woszczyk, A., Szypłowska, A., Lewandowski, A., Szerement, J., & Skierucha, W. (2020). Application of a monopole antenna probe with an optimized flange diameter for tdr soil moisture measurement. *Sens. Switz, 20*. https://doi.org/10.3390/s20082374

Mansouri-Far, C., Modarres Sanavy, S. A. M., & Saberali, S. F. (2010). Maize yield response to deficit irrigation during low-sensitive growth stages and nitrogen rate under semi-arid climatic conditions. *Agricultural Water Management, 97*, 12–22. https://doi.org/10.1016/j.agwat.2009.08.003

Martuza, M. A., Lee, C. H., Sazonov, A., Boumaiza, S., & Karim, K. S. (2018). Wireless LC-Type passive humidity sensor using large-area RF magnetron sputtered ZnO Films. *IEEE Transactions on Electron Devices, 65*, 3447–3453. https://doi.org/10.1109/TED.2018.2849706

Meder, F., Saar, S., Taccola, S., Filippeschi, C., Mattoli, V., & Mazzolai, B. (2021). Ultraconformable, self-adhering surface electrodes for measuring electrical signals in plants. *Adv. Mater. Technol., 6*, Article 2001182. https://doi.org/10.1002/admt.202001182

Mostajeran, A., & Rahimi-Eic, V. (2008). Drought stress effects on root anatomical characteristics of rice cultivars (oryza sativa L.). *Pakistan Journal of Biological Sciences, 11*, 2173–2183. https://doi.org/10.3923/pjbs.2008.2173.2183

Mulla, D. J. (2013). Twenty five years of remote sensing in precision agriculture: Key advances and remaining knowledge gaps. *Biosystems Engineering, 114*, 358–371. https://doi.org/10.1016/j.biosystemseng.2012.08.009

Nadler, A., Raveh, E., Yermiyahu, U., Lado, M., Nasser, A., Barak, M., & Green, S. (2008). Detecting water stress in trees using stem electrical conductivity measurements. *Soil Science Society of America Journal, 72*, 1014–1024. https://doi.org/10.2136/sssaj2007.0308

Nawaz, M., Sun, J., Shabbir, S., Khattak, W. A., Ren, G., Nie, X., Bo, Y., Javed, Q., Du, D., & Sonne, C. (2023). A review of plants strategies to resist biotic and abiotic environmental stressors. *The Science of the Total Environment, 900*, Article 165832. https://doi.org/10.1016/j.scitotenv.2023.165832

Nawazish, S., Hameed, M., & Naurin, S. (2006). Leaf anatomical adaptations of Cenchrusciliaris L. from the Salt Range, Pakistan against drought stress. *Pakistan Journal of Botany*, (38), 1723–1730.

Palazzari, V., Mezzanotte, P., Alimenti, F., Fratini, F., Orecchini, G., Virili, M., Mariotti, C., & Roselli, L. (2015). Leaf compatible eco-friendly temperature sensor clip for high density monitoring wireless networks. In *Mediterranean microwave symposium*. IEEE Computer Society. https://doi.org/10.1109/MMS.2015.7375456.

Palazzi, V., Bonafoni, S., Alimenti, F., Mezzanotte, P., & Roselli, L. (2019a). Feeding the world with microwaves: How remote and wireless sensing can help precision agriculture. *IEEE Microwave Magazine, 20*, 72–86. https://doi.org/10.1109/MMM.2019.2941618

Palazzi, V., Gelati, F., Vaglioni, U., Alimenti, F., Mezzanotte, P., & Roselli, L. (2019b). Leaf-Compatible autonomous RFID-based wireless temperature sensors for precision agriculture. In *2019 IEEE topical conference on wireless sensors and sensor networks (WiSNet)* (pp. 1–4). IEEE. https://doi.org/10.1109/WISNET.2019.8711808.

Pawlak, K., & Kołodziejczak, M. (2020). The role of agriculture in ensuring food security in developing countries: Considerations in the context of the problem of sustainable food production. *Sustain. Switz., 12*. https://doi.org/10.3390/su12135488

Pichorim, S. F., Gomes, N. J., & Batchelor, J. C. (2018). Two solutions of soil moisture sensing with rfid for landslide monitoring. *Sens. Switz., 18*. https://doi.org/10.3390/s18020452

Plavcová, L., & Jansen, S. (2015). The role of xylem parenchyma in the storage and utilization of nonstructural carbohydrates. In U. Hacke (Ed.), *Functional and ecological xylem anatomy* (pp. 209–234). Cham: Springer International Publishing. https://doi.org/10.1007/978-3-319-15783-2_8.

Sabiel, S. A. I., Abdelmula, A. A., Bashir, E. M. A., Yang, Y., Baloch, S. U., & Bashir, W. (2014). *Genetic variation of plant height and stem diameter traits in maize (Zea mays L.) under drought stress at different growth stages*.

Salmerón, J. F., Albrecht, A., Kaffah, S., Becherer, M., Lugli, P., & Rivadeneyra, A. (2018). Wireless chipless system for humidity sensing. *Sens. Switz., 18*. https://doi.org/10.3390/s18072275

Sarhadi, A. H., Hashemi, A., & Emami, H. (2013). Optimization of Q factor in complementary spiral resonator for RFID application. In *2013 21st telecommunications forum telfor (TELFOR). Presented at the 2013 21st telecommunications forum telfor (TELFOR)* (pp. 693–696). Belgrade, Serbia: IEEE. https://doi.org/10.1109/TELFOR.2013.6716323.

Sergienko, P., Kazmirenko, V., Chernov, A., & Prokopenko, Y. (2016). Q-factor of tuned microstrip resonator. *Radioelectronics and Communications Systems, 59*, 89–95. https://doi.org/10.3103/S0735272716020060

Seyfried, M. S., & Grant, L. E. (2007). Temperature effects on soil dielectric properties measured at 50 MHz. *Vadose Zone Journal, 6*, 759–765. https://doi.org/10.2136/vzj2006.0188

Sharma, A., Lang, R. H., Kurum, M., O'neill, P. E., & Cosh, M. H. (2020). L-band radar experiment and modeling of a corn canopy over a full growing season. *IEEE Transactions on Geoscience and Remote Sensing, 58*, 5821–5835. https://doi.org/10.1109/TGRS.2020.2971539

Singh, A., Pandey, H., Pandey, S., Lal, D., Chauhan, D., Aparna, Antre, S. H., B, S., & Kumar, A. (2023). Drought stress in maize: Stress perception to molecular response and strategies for its improvement. *Functional & Integrative Genomics, 23*, 296. https://doi.org/10.1007/s10142-023-01226-6

Stubbs, C. J., Larson, R., & Cook, D. D. (2022). Maize stalk stiffness and strength are primarily determined by morphological factors. *Scientific Reports, 12*, 720. https://doi.org/10.1038/s41598-021-04114-w

Tardieu, F., & Simonneau, T. (1998). Variability among species of stomatal control under fluctuating soil water status and evaporative demand: Modelling isohydric and anisohydric behaviours. *Journal of Experimental Botany, 49*, 419–432.

Ulaby, F., & El-rayes, M. (1987). Microwave dielectric spectrum of vegetation - Part II: Dual-dispersion model. *IEEE Transactions on Geoscience and Remote Sensing, GE-25*, 550–557. https://doi.org/10.1109/TGRS.1987.289833

Ulaby, F. T., & Jedlicka, R. P. (1984). Microwave dielectric properties of plant materials. *IEEE Transactions on Geoscience and Remote Sensing, GE-22*, 406–415. https://doi.org/10.1109/TGRS.1984.350644

USDA Agricultural Research Service, U.S.D.O.A.. (2015). *Germplasm resources information network (GRIN)*. https://doi.org/10.15482/USDA.ADC/1212393

Virdee, B. S., & Grassopoulos, C. (2003). Folded microstrip resonator. In *IEEE MTT-S international microwave symposium digest, 2003. Presented at the IEEE MTT-S international microwave symposium - ims 2003* (pp. 2161–2164). Philadelphia, PA, USA: IEEE. https://doi.org/10.1109/MWSYM.2003.1210591.

Wang, J., Chang, L., Aggarwal, S., Abari, O., & Keshav, S. (2020). Soil moisture sensing with commodity RFID systems. In *MobiSys 2020 - proceedings of the 18th international conference on mobile systems, applications, and services* (pp. 273–285). Association for Computing Machinery, Inc. https://doi.org/10.1145/3386901.3388940.

Wang, X., Deng, H., & Liu, C. (2018). High-Q sensor for permittivity detection based on spiral resonator. *Applied Physics A, 124*, 740. https://doi.org/10.1007/s00339-018-2152-x

Waseem, M., Mumtaz, S., Hameed, M., Fatima, S., Ahmad, M. S. A., Ahmad, F., Ashraf, M., & Ahmad, I. (2021). Adaptive traits for drought tolerance in red-grained wheat (Triticum *aestivum* L.) landraces. Arid Land Res. *OR Manager, 35*, 414–445. https://doi.org/10.1080/15324982.2021.1905103

Westgate, M. E., & Boyer, J. S. (1985). Osmotic adjustment and the inhibition of leaf, root, stem and silk growth at low water potentials in maize. *Planta, 164*, 540–549. https://doi.org/10.1007/BF00395973

Woszczyk, A., Szerement, J., Lewandowski, A., Kafarski, M., Szypłowska, A., Wilczek, A., & Skierucha, W. (2019). An open-ended probe with an antenna for the measurement of the water content in the soil. *Computers and Electronics in Agriculture, 167*. https://doi.org/10.1016/j.compag.2019.105042

Yan, Y. H., Lin, X. Q., Chen, Z., Cai, Y., & Chen, Z. (2020). A microwave sensor for leaf moisture detection based on split-ring resonator. In *Asia-pacific microwave conference proceedings, APMC* (pp. 427–429). Institute of Electrical and Electronics Engineers Inc.. https://doi.org/10.1109/APMC47863.2020.9331538

Yousaf, M. I., Riaz, M. W., Shehzad, A., Jamil, S., Shahzad, R., Kanwal, S., Ghani, A., Ali, F., Abdullah, M., Ashfaq, M., & Hussain, Q. (2023). Responses of maize hybrids to water stress conditions at different developmental stages: Accumulation of reactive oxygen species, activity of enzymatic antioxidants and degradation in kernel quality traits. *PeerJ, 11*, Article e14983. https://doi.org/10.7717/peerj.14983

Zhang, C., Kong, J., Wu, D., Guan, Z., Ding, B., & Chen, F. (2023). Wearable sensor: An emerging data collection tool for plant phenotyping. *Plant Phenomics, 5*, 51. https://doi.org/10.34133/plantphenomics.0051

Zhang, C., Marzougui, A., & Sankaran, S. (2020). High-resolution satellite imagery applications in crop phenotyping: An overview. *Computers and Electronics in Agriculture, 175*. https://doi.org/10.1016/j.compag.2020.105584

Zheng, L., Wang, Z., Sun, H., Zhang, M., & Li, M. (2015). Real-time evaluation of corn leaf water content based on the electrical property of leaf. *Computers and Electronics in Agriculture, 112*, 102–109. https://doi.org/10.1016/j.compag.2014.11.007